ELSEVIER

Chemical Engineering Journal 66 (1997) 1–10

CHEMICAL ENGINEERING JOURNAL

Local mass transfer and current distribution in baffled and unbaffled parallel plate electrochemical reactors

A.A. Wragg , A.A. Leontaritis

Chemical Engineering Group, School of Engineering, Exeter University, Exeter EX4 4QF, UK

Received 24 August 1994; accepted 17 June 1996

Abstract

Measurements of average and local mass transfer distributions were made in a parallel plate electrochemical cell using the limiting diffusion current technique based on ferricyanide ion reduction at nickel electrodes. The cell was operated with and without baffles. The local mass transfer coefficient values given by arrays of surface-flush mounted nickel mini-electrodes exhibited a distribution that reflected the complex hydrodynamics associated with phenomena such as cell inlet and exit effects and flow reversal at the baffles. In the unbaffled cell, the behaviour was dominated by a global swirling motion in the cell driven by the inlet jets. A relatively inactive zone appeared in the middle of the cell. Overall, the cell exhibited superior mass transfer performance when operated with baffles. The behaviour is compared with that in a similar cell described by Goodridge et al.

Keywords: Mass transfer; Parallel plate cell; Hydrodynamics; Electrochemical reactor; Baffles

1. Introduction

Parallel plate-type cells are a commonly used form of electrochemical reactor, in view of their ease of manufacture, electrode coating and assembly, their versatility for single-phase or multiphase processing, their adaptability to monopolar or bipolar operation, their relative uniformity of current distribution, and their flexible modularity, enabling additional cells to be added or removed from the stack. Membranes, or separators, can be easily incorporated and turbulence promoters can be included in the electrolyte space to enhance transport processes between the fluid and electrode surface. Knowledge of the current distribution and mass transfer performance is essential for the design and efficient operation of such cells.

An early example of work on mass transfer distribution in a parallel plate cell with a circular cross-section point of flow entry and a segmented electrode is the work of Pickett and Wilson [1], who identified a maximum mass transfer rate at a distance of approximately six equivalent diameters downstream of the cell entry. Earlier work from this laboratory [2] had explored axial and lateral wall mass transfer distributions in a parallel plate cell of square cross-section with a circular jet entry.

There are several examples of work in which the effect of turbulence promoters has been used to enhance the mass transfer rates in parallel plate cells [3–5]. More recently, Brown et al. [6] used segmented line electrodes, prepared using printed circuit board (PCB) technology, in an investigation of the local mass transfer behaviour in an ICI FMOI parallel plate electrolyzer with and without different types of net turbulence promoter. The same group [7] later studied space-averaged mass transfer and pressure drops with and without six different mesh-type turbulence promoters in the same cell geometry. In more recent work [8] from the same laboratory, the performance of a parallel cell modified by the incorporation of three-dimensional porous electrodes was studied and it was found that the operating current could be enhanced by a factor of 100 compared with the plane plate case.

Bakshi and Fedkiw [9] based their model for calculating the optimal time varying voltage control of an electrolyzer on the parallel plate model. This work considered the maximization of the yield of *p*-aminophenol by electroreduction of nitrobenzene in a reactor system operated in the batch recirculation mode.

A particularly novel use of the parallel plate geometry has been pioneered by Belmont and Girault [10,11], who used

PII S1385-8947(96)03148-X

interdigitated band electrodes produced by PCB screen-printing technology. This technique allows the reduction of the coplanar anode–cathode gap to a typical value of 250 μm, giving ohmic loss reduction of as much as 50% compared with conventional opposed parallel plate electrodes. The methoxylation of furan was successfully carried out in such a cell [11].

Interest in the relationship between a parallel plate cell geometry, the cell flow conditions and the electrochemical mass transfer performance continues [12–14], in an effort to enhance reactor performance and to obtain a greater understanding of the physical phenomena involved. The present investigation was prompted by the study of Goodrige and coworkers [15,16], who worked with a small and a large model of a baffled parallel plate cell with segmented electrodes. The fact that these workers used relatively large electrode segments precluded them from obtaining truly local values of the mass transfer coefficients. The purpose of the present work was to use surface-flush mini-electrodes in the cathode wall of a cell of the same dimensions as the smaller cell of Goodridge et al., with and without baffles in place, so that a detailed mapping of the mass transfer—and, hence, tertiary limiting current—distribution in such a cell might be obtained.

The method used here is the limiting diffusion current technique, which has been widely used in experimental mass and heat transfer determinations (see, for example, [17,18]). An earlier conference paper [19] has treated aspects of the present work, including a description of the experimental approach. However, it concentrated on a presentation of the average mass transfer performance of the cell. In the present paper, attention is focused on the segmental and local mass transfer behaviour as a function of the flow rate and baffle configuration.

2. Experimental details

The flow rig consisted of a centrifugal pump, an electrolyte reservoir of capacity 60 l, a water-cooled heat exchanger, a pair of rotameters and the horizontally oriented parallel plate cell. The rig is depicted in Fig. 1. Nitrogen cylinders were provided for electrolyte deoxygenation by sparging of the reservoir contents.

The cell, which is described in more detail elsewhere [19,20], consisted of two square nickel plates 3 mm thick and of face area 0.0225 m^2, which were separated by a PVC spacer frame of thickness 15 mm. The spacer frame was equipped with two baffles, the arrangement and detail of which are shown in Fig. 2(a) and 2(b). The electrolyte was introduced through three holes 5 mm in size situated in the PVC frame and followed a three-pass serpentine flow path through the cell. The inlet ports were located midway between the anode and cathode plates, and were separated by a lateral distance of 5 mm. The lateral distances between the port extremities and the cell wall and a line that represented an infinitely thin baffle were both 12.5 mm. The baffle openings were lozenge shaped, and were 20 mm long and 6 mm high. The baffle thicknesses were 3 mm. The nickel cathode and anode plates were set in a PVC block of thickness 15 mm. The overall geometry of this cell makes it almost identical to the smaller model used by Mamoor [16].

For the measurement of the local mass transfer rates, a 6 × 6 array of nickel mini-electrodes, each of diameter 1 mm, was inserted in three separate cathode plates in the cath-

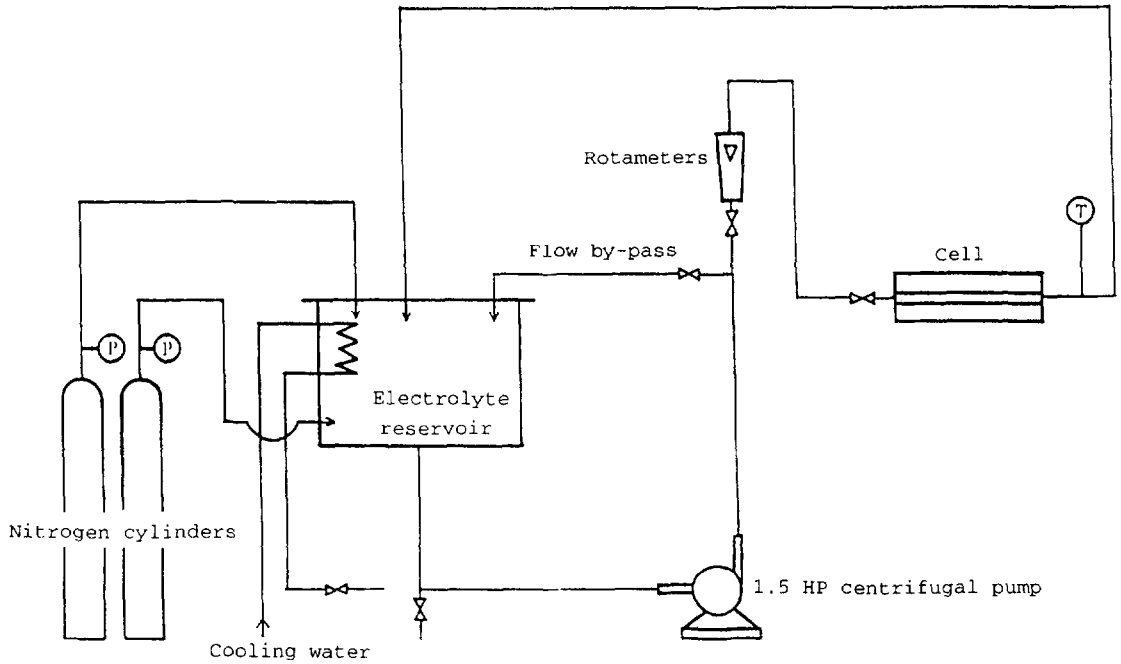

Fig. 1. Schematic diagram of flow rig.

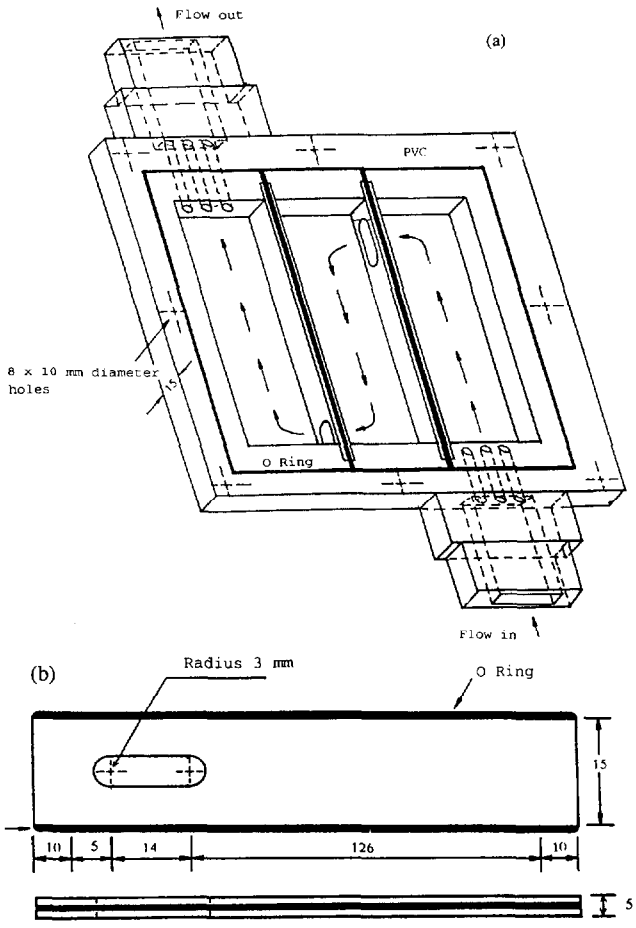

Fig. 2. (a) Perspective of cell frame and baffles and (b) detail of baffle, with dimensions in millimetres.

ode zones 1, 2 and 5 indicated in the insets of Figs. 6 and 7. The mini-electrodes were inserted with an 8.33 mm square pitch arrangement and were ground flush with the surface of the main cathode plate to ensure hydrodynamic smoothness. By appropriate rotation of the cathode plate on assembly, these three instrumented zones allowed mapping of the entire plate surface (i.e. all zones 1–9), with a total of 324 measuring points being available. Each mini-electrode was electrically isolated from the main cathode, being fixed with Araldite 2004. A photograph of a cathode plate with mini-electrodes inserted in the upper flank zone is shown in Fig. 3.

Fig. 4 depicts the electrical circuit and instrumentation used for the measurement of current from the local cathodes. The test and main cathodes were maintained at an identical fixed potential of −850 mV relative to the anode; this potential was known to correspond to the mid-plateau region of the current–voltage curves (see Fig. 5). Thus, all the potentials are quoted relative to the potential of the anode. This two-electrode technique is adequate where a true measurement of the cathode potential is not required—only the location of the plateau region. The currents were measured and recorded on a data acquisition system (DAS) designed and constructed in house. This DAS was capable of reading and averaging the fluctuating signals from up to 32 channels scanned at a frequency of 100 Hz over a period of 60 s.

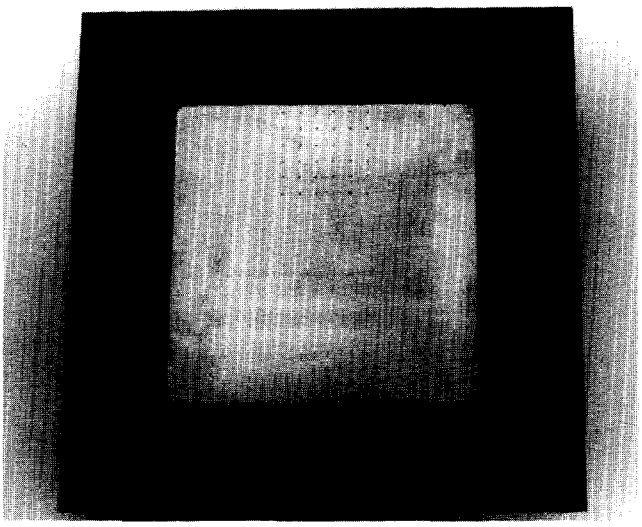

Fig. 3. Cathode plate showing mini-electrodes in upper flank region.

The electrolyte was an aqueous solution of 0.005 M ferricyanide, 0.01 M potassium ferrocyanide and 0.5 M sodium hydroxide, which was made up in water using AnalaR reagents and distilled water. The ferrocyanide concentration was double the ferricyanide concentration, to ensure that the limiting reaction would be at the cathode, with the electrode areas being equal in this case. The electrolyte was deoxygenated using N_2 bubbling in the bulk tank and the maintenance of a N_2 blanket at all times. Light was excluded from the rig as far as possible. The temperature was maintained at 20 ± 0.5 °C by means of a water-cooled glass cooling coil in the bulk tank. The ferricyanide ion concentration was measured by UV spectrophotometry prior to and following each day's experiments. The physical properties of the electrolyte at 20 °C are listed in Table 1.

The mass transfer coefficients were calculated using the relationship

$$k = \frac{I_{LIM}}{zFA_e c_\infty} \quad (1)$$

Examples of typical current–potential curves obtained for one mini-electrode at different cell Reynolds numbers are shown in Fig. 5. It can be seen that the plateau region of the plots is extremely well defined, so enabling accurate reading of the limiting current for use in Eq. (1).

3. Results

3.1. Average mass transfer coefficients

The average mass transfer data from the entire cathode plate (macrocathode) have been reported elsewhere [19]. In summary, for the baffled cell, the data were well correlated by the equation

$$Sh = 0.46\, Re^{0.66}\, Sc^{0.33} \quad (2)$$

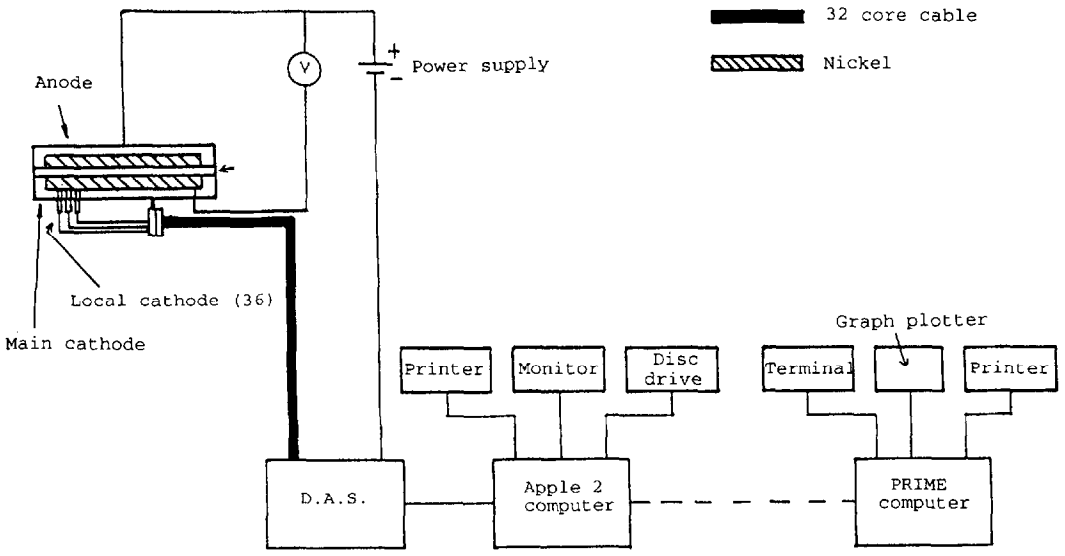

Fig. 4. Electrical circuit.

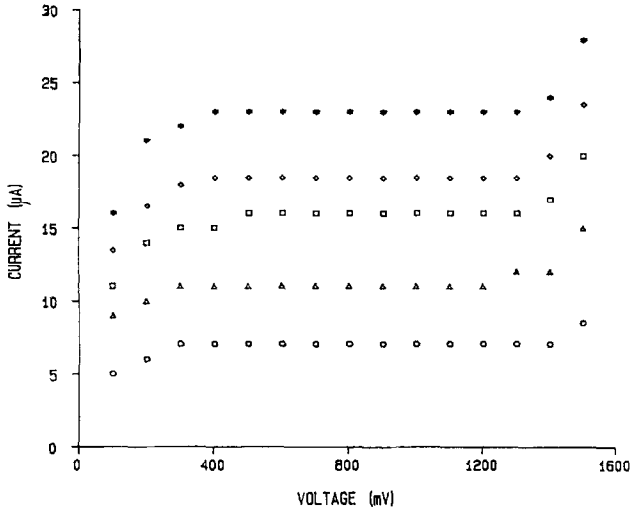

Fig. 5. Current–voltage curves for a selected mini-electrode for baffled cell: ○, Re = 2510; △, Re = 5700; □, Re = 8800; ◇, Re = 12 200; *, Re = 16 600.

Table 1
Physical properties of electrolyte at 20 °C

Concentration of $Fe(CN)_6^{3-}$ (M)	0.005
Concentration of $Fe(CN)_6^{4-}$ (M)	0.01
Concentration of NaOH (M)	0.50
Density ρ (kg m^{-3})	1020.5
Viscosity μ (kg m^{-1} s^{-1})	1.105×10^{-3}
Diffusivity D of $Fe(CN)_6^{3-}$ (m^2 s^{-1})	6.631×10^{-10}
Schmidt number Sc	1633

in the range $3 \times 10^3 < Re < 1.5 \times 10^4$, i.e. the turbulent regime. Here, the Reynolds number is based on the hydraulic mean diameter of one channel of the cell. The present data lie a few per cent lower than those of Goodridge et al. [15], possibly as a result of the discontinuous, segmented nature of their electrodes producing a small degree of hydrodynamic disturbance.

The average data for the unbaffled cell were well correlated by the equation

$$Sh = 0.19\, Re^{0.812}\, Sc^{0.33} \quad (3)$$

in the range $1.25 \times 10^3 < Re < 6.9 \times 10^3$. The baffled cell data lie some 25%–30% above those for the unbaffled case. Goodridge et al. did not report results for the unbaffled condition, so a comparison is not possible. The difference in the exponents on the Reynolds number between Eq. (2) and (3) is indicative of different hydrodynamic regimes: this is discussed in more detail later.

3.2. Zonal mass transfer distribution: baffled cell

Figs. 6 and 7 show the variation of zonal averaged mass transfer coefficients that correspond to the segment numbers given on the right-hand side of the figures for two different Reynolds numbers. A comparison is made with Goodridge et al. [15], whose data were simply obtained from the current value given by a particular segment. The present data were obtained by averaging readings from the 36 mini-electrodes situated in each segment of our plane plate.

It can be seen that the mass transfer rate, as given by $Sh\, Sc^{-0.33}$, is highest at the inlet segment, as a result of the strong effect of the turbulent, interacting jets from the inlet ports [2,17]. The mass transfer rate then decays between segments 1 and 3 as flow development takes place. The hydrodynamic disturbance caused by the flow changing direction and flowing through the baffle, which produces another jet effect, causes a significant increase in Sh between segments 3 and 4. Flow development then takes place again between segments 4 and 6, before the baffle effect again produces an enhancement between segments 6 and 7. Along the final section of the flow path, a mass transfer reduction occurs between segments 7 and 8, followed by an enhancement at segment 9 that results from flow disturbance caused by the cell outlet.

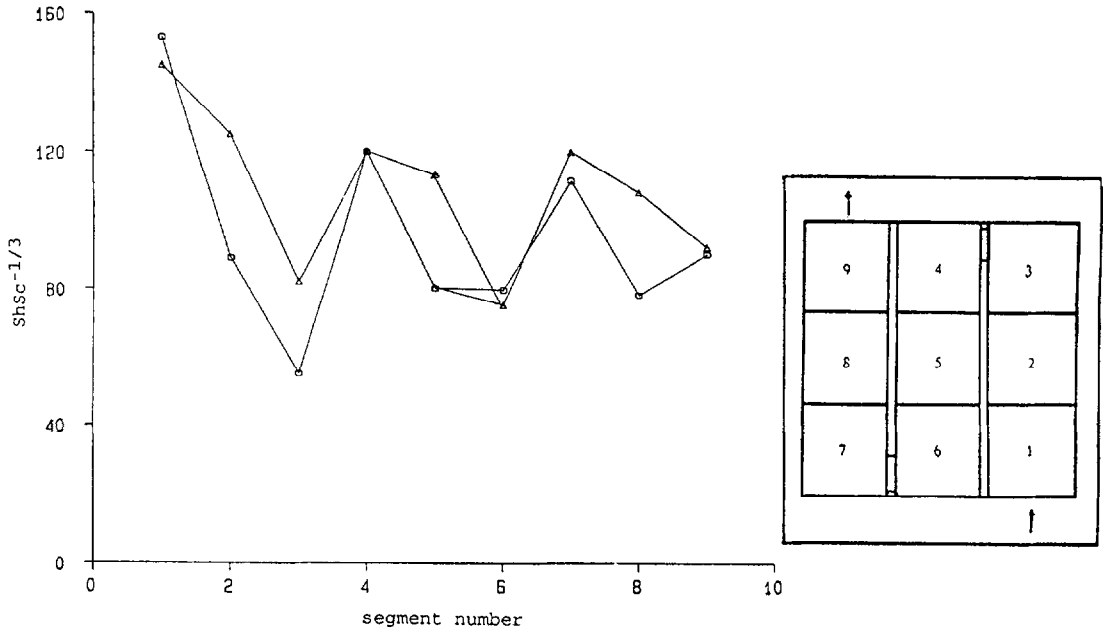

Fig. 6. Segmental Sh $Sc^{-1/3}$ distribution for baffled cell for Re = 3900: O, present; Δ, Goodridge et al. [15].

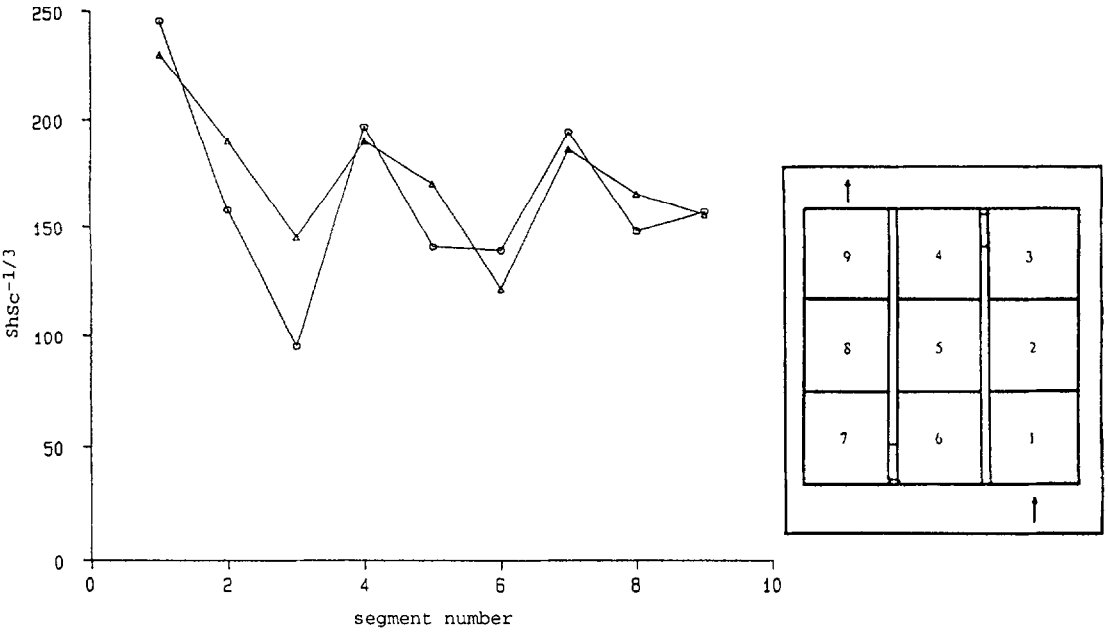

Fig. 7. Segmental $ShSc^{-1/3}$ distribution for baffled cell for Re = 8400: O, present; Δ, Goodridge et al. [15].

These findings can be seen to be in broad agreement with those of Goodridge et al., except for the rise in Sh at the final segment, which is a plausible phenomenon, consistently identified in the present work.

3.3. Local mass transfer distribution: baffled cell

The local mini-electrode data provided by the 324 measuring points give much greater detail for the mass transfer coefficient distribution and allow us to make inferences regarding the hydrodynamic conditions at various points in the cell. It should be noted that the local mass transfer coefficient distribution is directly related to the tertiary (limiting) current distribution in such a cell.

The discussion follows data that correspond to the flow path lines indicated in the right-hand side of each of Figs. 8-13. Fig. 8 shows k values in the first channel of the baffled cell at Re = 15 700. For each of the flow paths, k is high immediately following the cell inlet and rises to a peak value some 30–40 mm into the cell. The occurrences of such peak mass and/or heat transfer rates downstream of jet inlets has been well documented in the literature (see, for example, [1,2,17]). Hydrodynamic development then occurs, with growth of the mass transfer boundary layer and consequent

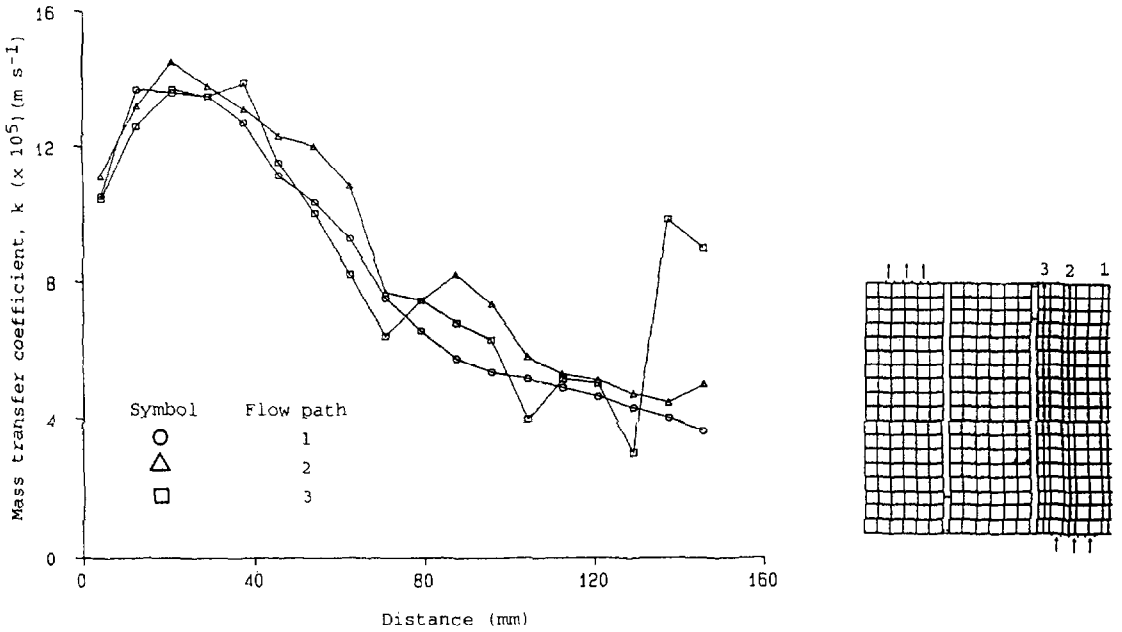

Fig. 8. Local mass transfer coefficient distribution for three flow paths in channel 1 with Re = 15 700: ○, flow path 1; △, flow path 2; □, flow path 3.

decay of k. Along flow path 3, there is a large increase in k immediately in front of the baffle opening.

Fig. 9 charts k distributions affected by the passage of electrolyte through the first baffle opening at Re = 15 700. For the first five measuring points upstream of the baffle, the k values are low and similar. The flow through the baffle, with its consequent disturbance of the flow, causes a large increase in k, especially along flow paths 2 and 3. A further rise in k for mini-electrode 12 is evident along all flow paths as the jet from the baffle opening impinges on the second baffle well.

For flow down the second channel, Fig. 10 illustrates an important effect. It can be seen that the k values on the left-hand side of the channel (flow path 3) are massively higher than those on the right-hand side (flow path 1), especially in the upper part of the figure. Clearly, fluid is preferentially channelling down the left-hand side as it emerges from the baffle. Equalization of the flow to give roughly equal k values occurs with increasing distance downstream. Flow path 3 again experiences a large increase in k immediately in front of the second baffle. Such detailed information regarding the k distribution and associated hydrodynamics was not available from the study of Goodridge [15].

The behaviour for the selected family of flow paths that pass through the second baffle opening is shown in Fig. 11. Again, the values are fairly similar for the first five electrodes

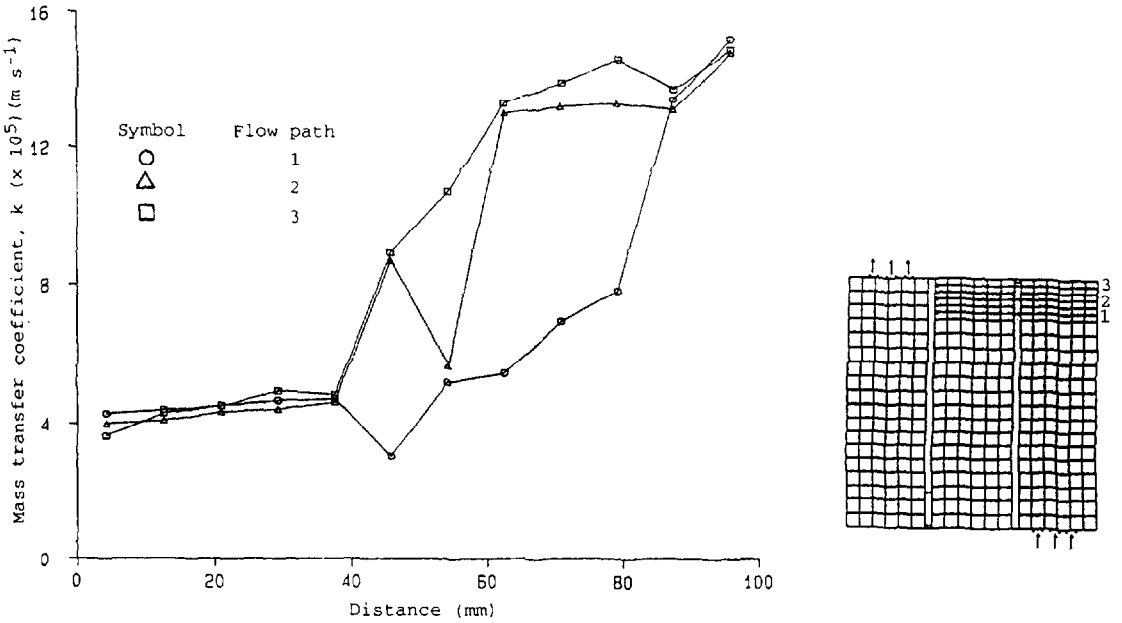

Fig. 9. Local mass transfer coefficient distribution for three flow paths between channels 1 and 2 with Re = 15 700: ○, flow path 1; △, flow path 2; □, flow path 3.

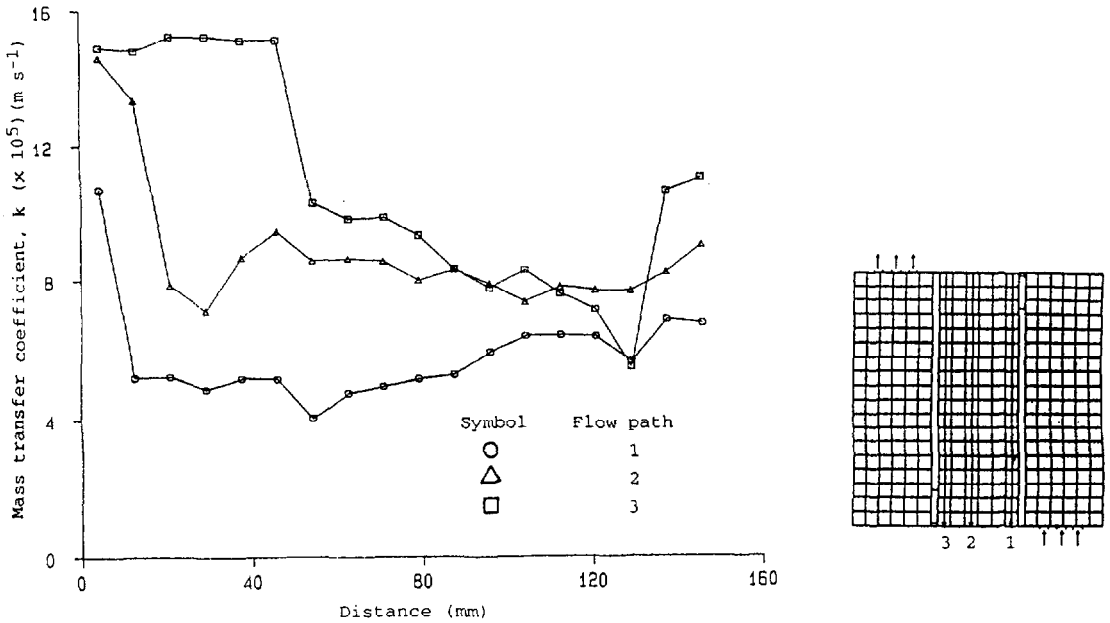

Fig. 10. Local mass transfer coefficient distribution for three flow paths in channel 2 with Re = 15 700: ○, flow path 1; △, flow path 2; □, flow path 3.

but passage through the baffle opening produces another major disturbance, and the k values are significantly enhanced for flow paths 1 and 2 as the electrolyte scours around the upstream head of channel 3. Also, the impact of the baffle jet on the cell side wall produces roughly similar k values at the 12th mini-electrodes with a large increase in the value for flow path 3.

Flow up the third channel leading to the exit is represented in both Figs. 12 and 13 for widely different channel Reynolds numbers of 2510 and 15670 respectively. In both figures, there is again evidence of preferential flow up the left-hand side of the channel, producing larger k values (flow path 3) than those on the right-hand side (flow path 1). However, the flow equalizes as the distance downstream increases and there is evidence of an up-turn in local k values in the vicinity of the exit ports—this finding is consistent with that represented for the zonal data in Figs. 6 and 7.

3.4. Local mass transfer distribution: unbaffled cell

With the baffles removed, the existence of over 300 data points without intervening walls constituted an ideal scenario for the use of a contour plotting routine to produce iso-k profiles. The resultant contour plots for cell Reynolds numbers of 1830 and 3269 are shown in Figs. 14 and 15 respec-

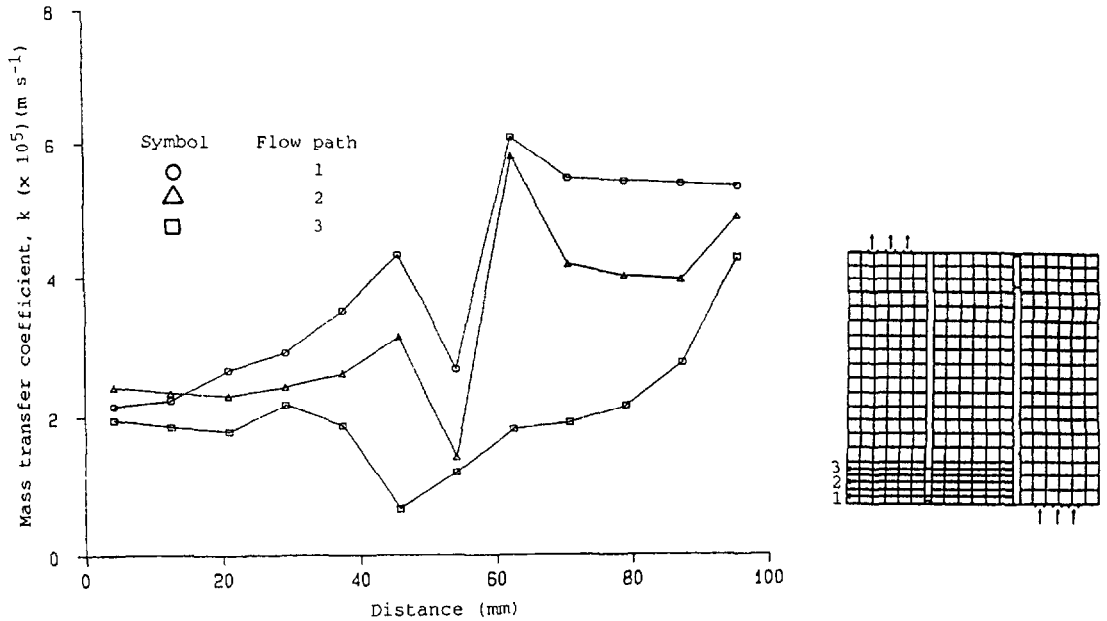

Fig. 11. Local mass transfer coefficient distribution for three flow paths between channels 2 and 3 with Re = 2510: ○, flow path 1; △, flow path 2; □, flow path 3.

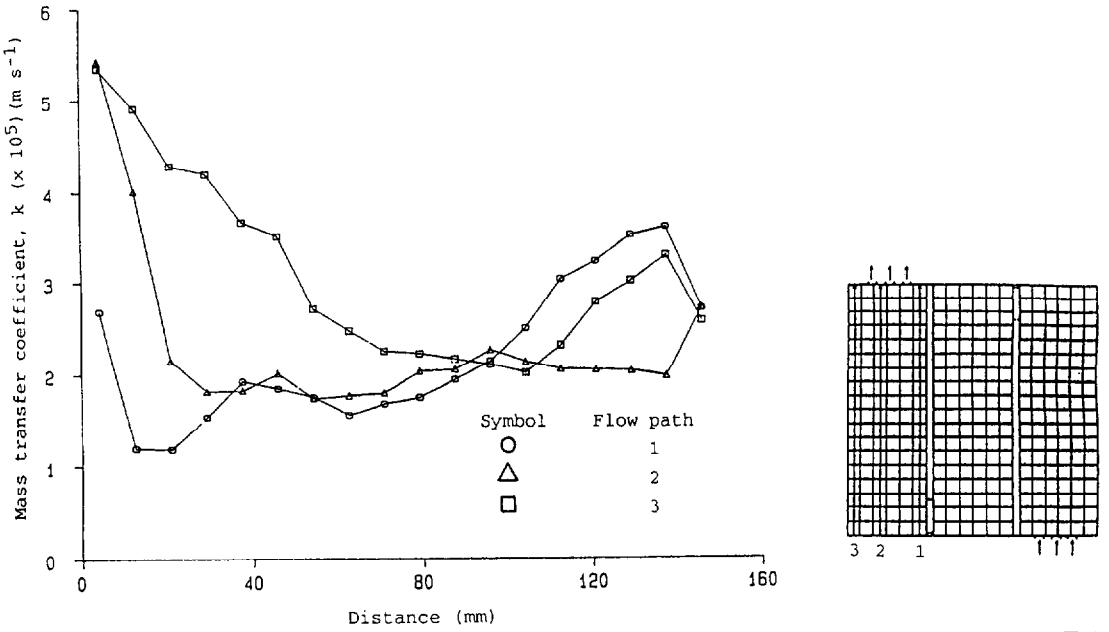

Fig. 12. Local mass transfer coefficient distribution for three flow paths in channel 3 with Re = 2510: ○, flow path 1; △, flow path 2; □, flow path 3.

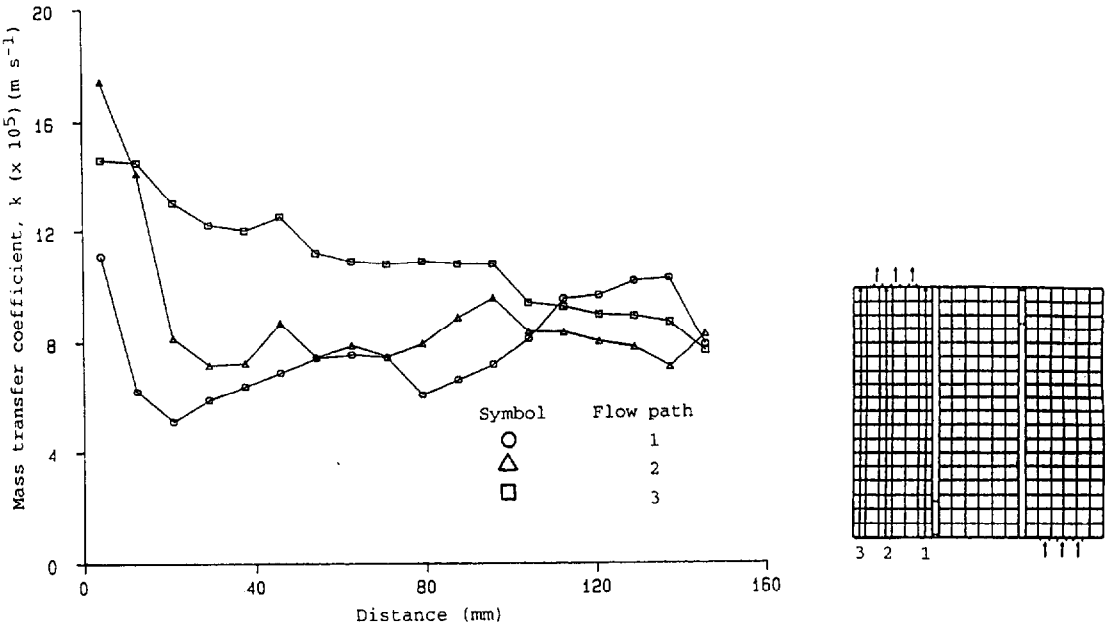

Fig. 13. Local mass transfer coefficient distribution for three flow paths in channel 3 with Re = 15 700: ○, flow path 1; △, flow path 2; □, flow path 3.

tively. A further, similar, plot was given elsewhere [19] for Re = 5492.

The plots are dominated by two features. First, the low values of k in the centre of the plate and the generally high values around the perimeter are indicative of a predominantly swirling motion around the cell driven by the inlet jets. Thus, in the centre of the cell for Re = 1830, the local mass transfer coefficient is only $5 \times 10^{-6}\,m\,s^{-1}$, whereas it reaches values as high as 4.5×10^{-5} m s^{-1} around the edge. Secondly, there are very steep gradients of k where the swirling motion in the cell and the entry jets interact. As seen earlier, when comparing the global performance of the baffled and unbaffled cells, the baffled cell gives superior mass transfer values, largely as a result of the avoidance of the central dead zone in the unbaffled cell. Further flow visualization studies with a transparent-sided cell confirmed the circulatory motion of the electrolyte in the unbaffled cell [21].

4. Conclusions

The use of the limiting diffusion technique with surface flush-mounted mini-electrodes has enabled us to carry out detailed mapping of the local mass transfer distributions in parallel plate electrochemical cells with and without baffles. In the baffled cell, a wide range of complex and interacting

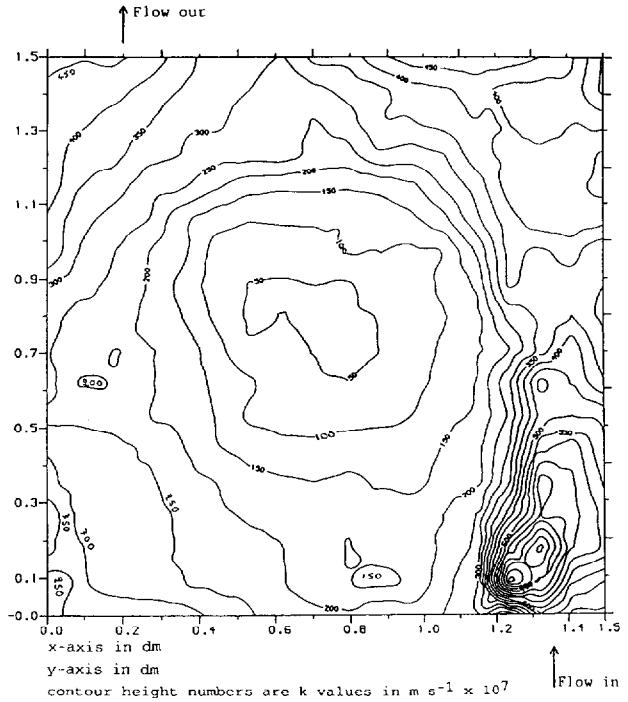

Fig. 14. Contour plots of local mass transfer coefficient distribution in the unbaffled cell with Re = 1830. Both axes are in decimetres and contour height numbers are k values (in m s^{-1} × 10^7).

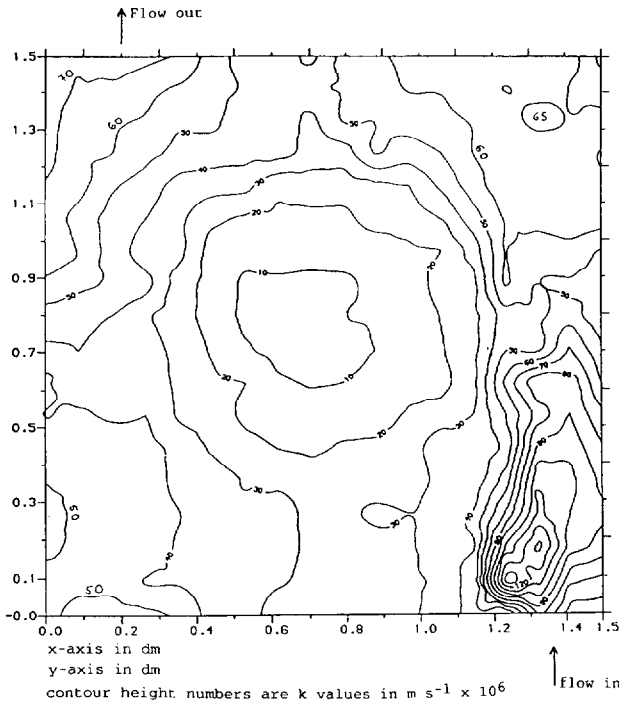

Fig. 15. Contour plots of local mass transfer coefficient distribution in the unbaffled cell with Re = 3270. Both axes are in decimetres and contour height numbers are k values (in m s^{-1} × 10^6).

hydrodynamic phenomena, including jet entry effects, recirculation zone peaking, flow development, flow reversal, wall impingement, preferential flow effects and exit disturbances, have been shown to exist and to effect the mass transfer distribution. In the unbaffled situation, a swirling motion in the cell results in a relatively dead zone in the centre, and generally high activity around the edges. The overall average performance of the baffled cell is superior to that of the unbaffled cell. This study has yielded working correlations for the overall mass transfer performance, while also highlighting the large local variations in the tertiary current density that exist in such cells, which might result in phenomena such as preferential wear of electrode coatings with processes under mass transfer control.

One final point concerns the turbulence levels in the baffled cell. Several workers have effectively used net- and mesh-type turbulence promoters to enhance the mass transfer rates in parallel plate cells (see, for example, [3–5]). Further work by Hastings [21,22], who used a variety of 'turbulence-enhancing' devices, produced negative results in all cases; i.e. the mass transfer rates were actually decreased with respect to those for the unmodified channels. This highlights the fact that the behaviour of the present, relatively short, cell is dominated by turbulence produced by the inlet jets and the sudden changes in flow direction. The incorporation of nets and meshes simply served to damp naturally occurring turbulence and block available electrode surface area. Thus, cell design should take account of inherent turbulence levels before the possible deployment of turbulence promoters is considered.

Appendix A. Nomenclature

A_e	electrode area (m^2)
A_x	flow cross-sectional area of channel or cell (m^2)
C_∞	bulk concentration of reacting ions (mol m^{-3})
D	diffusion coefficient (m^2 s^{-1})
d_H	hydraulic mean diameter of channel or cell ($4A_x/P$) (m)
I_{LIM}	limiting current (A)
F	Faraday number (C mol^{-1})
k	mass transfer coefficient (m s^{-1})
P	wetted perimeter of channel or cell (m)
u	mean channel velocity (m s^{-1})
z	number of electrons exchanged (—)

Dimensionless groups

Sc	Schmidt number ($\mu/\rho D$)
Sh	Sherwood number (kd_H/D)
Re	Reynolds number ($d_H u\rho/\mu$)

Greek letters

μ	dynamic viscosity of electrolyte (kg m^{-1} s^{-1})
ρ	density of electrolyte (kg m^{-3})

References

[1] D.J. Pickett and C.J. Wilson, *Electrochim. Acta, 27* (1982) 591.
[2] A.A. Wragg, D.J. Tagg and M.A. Patrick, *J. Appl. Electrochem., 10* (1980) 43.

[3] F. Schwager, P.M. Robertson and N. Ibl, *Electrochim Acta, 25* (1980) 1655.
[4] F.B. Leitz and L. Marincic, *J. Appl. Electrochem., 7* (1977) 473.
[5] A. Storck and B. Hutin, *Electrochim. Acta, 26* (1981), 127.
[6] C.J. Brown, D. Pletcher, F.C. Walsh, J.K. Hammond and D. Robinson, *J. Appl. Electrochem., 22* (1992) 613.
[7] C.J. Brown, D. Pletcher, F.C. Walsh, J.K. Hammond and D. Robinson, *J. Appl. Electrochem., 23* (1993) 38.
[8] C.J. Brown, D. Pletcher, F.C. Walsh, J.K. Hammond and D. Robinson, *J. Appl. Electrochem., 24* (1994) 95.
[9] R. Baskshi and P.S. Fedkiw, *J. Appl. Electrochem., 24* (1994) 1116.
[10] C. Belmont and H.H. Girault, *J. Appl. Electrochem., 24* (1994) 475.
[11] C. Belmont and H.H Gerault, *J. Appl. Electrochem., 24* (1994) 719.
[12] D.A. Szanto, P. Trinidad and F.C. Walsh, *Proc. 4th Euro. Symp. on Electrochemical Engineering (CHISA), Prague*, 1996.
[13] W.M. Taama, R.E. Plimley and K. Scott, *Proc. 4th Euro. Symp. on Electrochemical Engineering (CHISA), Prague*, 1996.
[14] C. Bengoa, A. Montillet, P. Legentilhomme and J. Legrand, *J. Appl. Electrochem.*, in press.
[15] F. Goodridge, G.M. Mamoor and R.E. Plimley, *Inst. Chem. Eng. Symp. Ser.. 98* (1985) 61.
[16] G.M. Mamoor, *Ph.D. Thesis*, University of Newcastle on Tyne, 1983.
[17] D.J. Tagg, M.A. Patrick and A.A. Wragg, *Trans. Inst. Chem. Eng., 57* (1979) 176.
[18] S. Yapici, M.A. Patrick and A.A. Wragg, *J. Appl. Electrochem,. 24* (1994) 685.
[19] A.A. Wragg and A.A. Leontaritis, in *Electrochemicaal Cell Design and Optimisation, Dechema Monograph, 123* (1991) 345.
[20] A.A. Leontaritis, *M. Phil. Thesis*, University of Exeter, 1988.
[21] M.W. Hastings, *Project Rep.*, School of Engineering, University of Exeter, 1993.
[22] A.A. Wragg and M.W. Hastings, *Abstracts 45th Meet. of the International Society of Electrochemistry, Porto*, 1994.